NANO LETTERS

Letter

pubs.acs.org/NanoLett

Ultrahigh Torsional Stiffness and Strength of Boron Nitride Nanotubes

Jonathan Garel,[†] Itai Leven,[‡] Chunyi Zhi,[§] K.S. Nagapriya,[†,⊥] Ronit Popovitz-Biro,[∥] Dmitri Golberg,[§] Yoshio Bando,[§] Oded Hod,[‡] and Ernesto Joselevich*[,†]

[†]Department of Materials and Interfaces, Weizmann Institute of Science, Rehovot 76100, Israel

[‡]School of Chemistry, The Sackler Faculty of Exact Sciences, Tel Aviv University, Tel Aviv 69978, Israel

[§]International Center for Materials Nanoarchitectonics (MANA), National Institute for Materials Science (NIMS), Namiki 1-1, Tsukuba, Ibaraki 305-0044, Japan

[∥]Chemical Research Support, Weizmann Institute of Science, Rehovot 76100, Israel

S *Supporting Information*

ABSTRACT: We report the experimental and theoretical study of boron nitride nanotube (BNNT) torsional mechanics. We show that BNNTs exhibit a much stronger mechanical interlayer coupling than carbon nanotubes (CNTs). This feature makes BNNTs up to 1 order of magnitude stiffer and stronger than CNTs. We attribute this interlayer locking to the faceted nature of BNNTs, arising from the polarity of the B−N bond. This property makes BNNTs superior candidates to replace CNTs in nanoelectromechanical systems (NEMS), fibers, and nanocomposites.

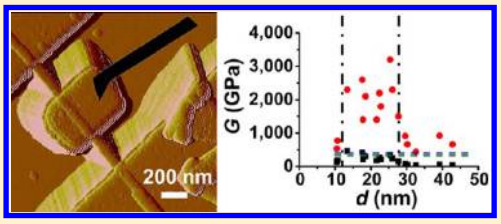

KEYWORDS: *Nanotube, boron nitride (BN), atomic force microscopy (AFM), torsion, nanomechanics, faceting*

Carbon nanotubes (CNTs) are, together with graphene, the stiffest and strongest material discovered so far, in terms of both elastic modulus and tensile strength.[1,2] They have therefore been considered prime components for fibers,[3] nanocomposites,[4] and nanoelectromechanical systems (NEMS).[5] However, these outstanding mechanical properties, valid for one single layer, are hard to exploit at larger scales because the weak shear interactions between adjacent layers[6−8] in multiwall CNTs or CNT bundles markedly decreases their effective stiffness and strength.[3,9] CNT-based fibers have still to match the mechanical resistance of Kevlar or polyethylene fibers.[3] In nanoresonators based on multiwall CNTs, interwall sliding induces internal friction,[10] which leads to energy dissipation, loss of sensitivity, and to a decrease of the quality factor,[11,12] as compared for instance with inorganic nanowires.[13] There is therefore a need for stiffer layered materials with stronger interlayer coupling for such applications.

The mechanical response of multiwall nanotubes to torsion provides a direct measure of their interlayer coupling.[7,8,14,15] The torsional behavior of multiwall CNTs[7,8] and WS_2 nanotubes[15] has already been investigated, showing qualitatively different responses. Upon application of a torque to a multiwall CNT, only the outer layer twists, slipping around the inner layers.[7,8] Conversely, a WS_2 nanotube behaves as a strongly coupled system where all layers contribute to the mechanical properties, up to a critical torsion angle, beyond which a stick−slip behavior of the outer layer around the inner layers is observed.[15] Nevertheless, the individual WS_2 layers are relatively soft (Young's modulus of about 150 GPa,[16] compared to 1 TPa for CNTs);[2] thus, the strong interlayer coupling is not sufficient to make WS_2 nanotubes stiffer than CNTs.

Boron nitride nanotubes (BNNTs)[17,18] are expected to benefit both from a high stiffness, like CNTs, and a high interlayer coupling, like WS_2 nanotubes. On the one hand, BNNTs have a Young's modulus similar to that of CNTs,[18] thus making them at least as stiff as CNTs. On the other hand, the polar nature of the B−N bond could favor interlayer electrostatic interactions and thus significantly increase the mechanical coupling between adjacent layers as compared with CNTs. Indications of this expected high interlayer interaction can be seen in the eclipsed stacking arrangement of B and N atoms in bulk hexagonal boron nitride (*h*-BN)[18] and in the correlation between chiralities of different layers in multiwall BNNT.[18,19] Additionally, it has been shown that whereas the spacing between two layers of *h*-BN is controlled by van der Waals forces, their sliding energy is governed by electrostatic interactions through Pauli repulsion.[20] On the basis of the understanding that their mechanical properties should be dictated by the correlated contributions of all the layers, we hypothesized that BNNTs should be effectively stiffer and stronger than CNTs.

To test this hypothesis, we have performed the first experimental study of BNNT torsional mechanics. BNNTs were synthesized by chemical vapor deposition as previously described.[21,22] The measurements were performed on BNNT

Received: September 27, 2012
Revised: November 1, 2012
Published: November 6, 2012

   dx.doi.org/10.1021/nl303601d | *Nano Lett.* 2012, 12, 6347−6352

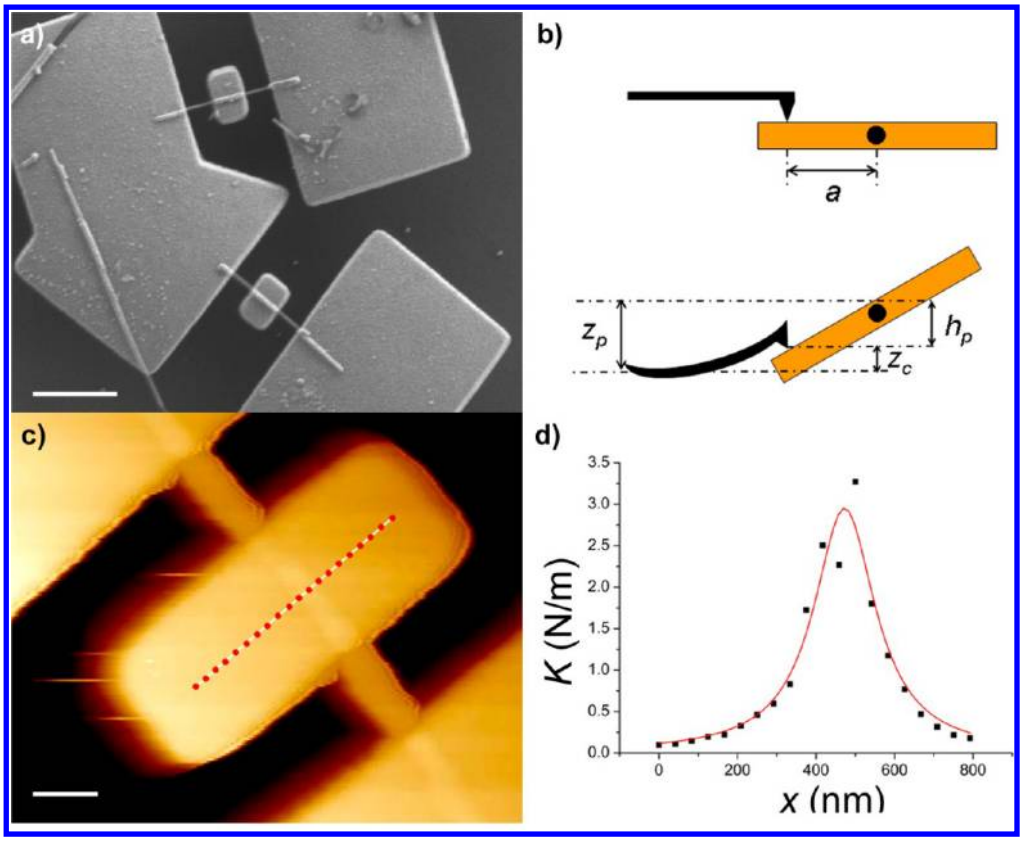

Figure 1. Measurement of BNNT torsional spring constant. (a) Scanning electron microscopy (SEM) images of two suspended BNNT torsional devices. Scale bar: 1 μm. (b) Schematic description of the cantilever and pedal during a force−distance measurement. a is the lever arm from the axis of the nanotube, z_p is the z-piezo extension, $h_p = z_p - z_c$ is the deflection of the pedal, and z_c is the deflection of the cantilever. (c) AFM tapping mode height image of a suspended BNNT with a pedal. The red dots correspond to points where we acquire a force−distance measurement. Scale bar: 200 nm. (d) Linear stiffness plotted as a function of the position along the pedal (first measurement point is set to zero by definition). The data were fitted to eq 1 (see text).

torsional devices similar to those that we have previously used to twist carbon[8,14] and WS_2 nanotubes.[15] These devices consist of a suspended BNNT clamped between metallic pads, with a pedal located on top of it (Figure 1a). They were fabricated using electron-beam lithography, followed by wet etching and critical point drying (see Supporting Information for details). The BNNTs were twisted by pressing against the pedal with an atomic force microscope (AFM) tip. By measuring the deflection of the AFM tip, the force exerted on the pedal was determined.[7,8]

As a first step, we determined the torsional spring constant of BNNTs (Table S1) by pressing at different points along the long axis of the pedal. For each point, we measured the linear stiffness K of the system, calculated as $K = k_c z_c/(z_p - z_c)$, where k_c is the spring constant of the cantilever, z_p is the z-piezo extension, and z_c is the deflection of the cantilever[7,8] (Figure 1b). K was plotted as a function of the position along the pedal and fitted to

$$K = \left[\frac{(x-a)^2}{2\kappa} + {K_B}^{-1}\right]^{-1} \quad (1)$$

where x is the distance measured along the pedal (see white−red line in Figure 1c), the torsional spring constant (κ), the bending spring constant (K_B), and the lever arm (a) being left as floating parameters.[7] This method enables us to separate the contributions to the pedal deformation that are lever arm dependent (twisting) from those that are lever arm independent (bending and slack). The linear stiffness increases as we press closer to the torsional axis (i.e., to the center of the nanotube), then reaches a maximum, and decreases as we press further away (Figure 1d and Figure S1). This is a manifestation of Archimedes law of the lever and clearly indicates that the nanotube is twisting. All curves could be fitted to eq 1 with good accuracy.

The torsional spring constant κ depends not only on the number of layers that carry the torque applied to the external wall of the nanotube but also on the diameter and suspended length of the BNNT. Therefore, κ cannot be directly used to characterize BNNT torsional stiffness. The shear modulus G, on the other hand, is an intrinsic characteristic of the nanotube that provides a measure for its stiffness. Classical elasticity theory gives $G = 2\kappa L/[\pi({r_{out}}^4 - {r_{in}}^4)]$, where L is the length of the suspended segments of the BNNT and r_{in} and r_{out} are the inner and outer radii of the cylinder, respectively.[7,15] (Although r_{in} is not directly accessible to our measurements, transmission electron microscopy (TEM) images show that r_{in} is usually about half of r_{out}. Therefore, ${r_{in}}^4 \ll {r_{out}}^4$, and the inner radius r_{in} can be neglected.) In order to determine the degree of mechanical coupling between layers, we calculated, for each BNNT, two boundary values for the effective shear modulus, corresponding to two extreme possible cases. (i) Solid rod: in this case interwall torsional coupling is assumed to be infinite, so that all the walls are locked and twist together, yielding $G_s = 2\kappa L/(\pi {r_{out}}^4)$. (ii) Hollow cylinder: here, the torsional coupling is assumed to be negligible and the outer wall twists and slides

dx.doi.org/10.1021/nl303601d | Nano Lett. 2012, 12, 6347−6352

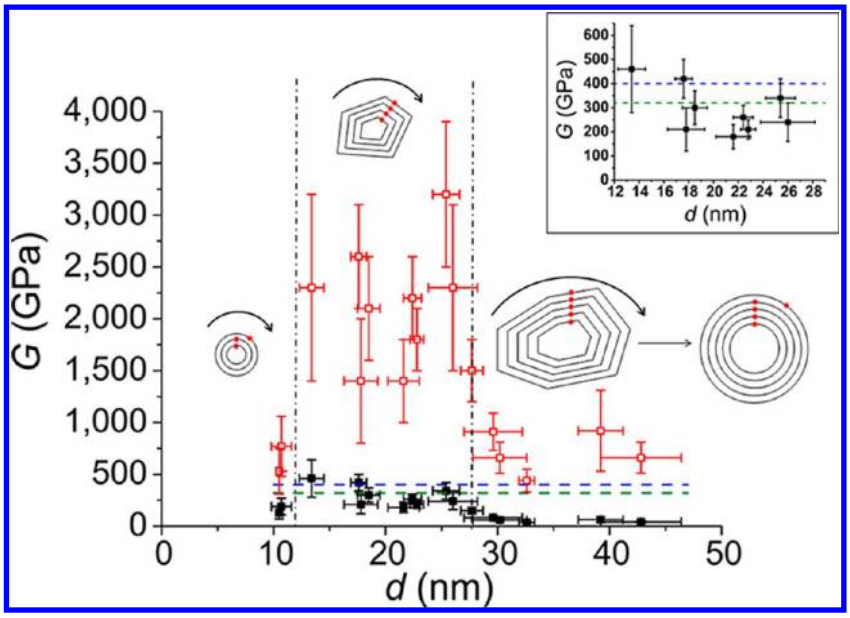

Figure 2. Effective shear modulus as a function of nanotube diameter, according to solid-rod (black) and hollow-cylinder cases (red) (see text). Blue dashed line: theoretical shear modulus of single-wall BNNT.[23] Green dashed line: experimental shear modulus of *h*-BN.[24] Schematic cartoons illustrating BNNT torsional behavior are presented: circular cross section and low torsional coupling for thin BNNTs (d < 12 nm), faceted cross section and high torsional coupling for intermediate diameters (d = 12−27 nm), faceted cross section, unfaceting under torsional stress and low torsional coupling for thick BNNTs (d > 27 nm) (see text). Inset: close-up of the "solid rod" shear modulus for intermediate diameters, where ultrahigh stiffness occurs. Horizontal and vertical error bars correspond to the standard deviation of the experimental data (see Supporting Information for details).

freely around the inner walls. In that case, $r_{out} - r_{in} = \delta r$ = 3.4 Å, where δr is the interlayer distance, and then $G_h = 2\kappa L/(4\pi r_{out}{}^3 \delta r)$. Comparing G_s and G_h to the theoretical shear modulus G_{th}(BNNT) = 400 GPa[23] and the experimental shear modulus of hexagonal boron nitride G_{exp}(*h*-BN) = 320 GPa,[24] used as reference values, enables us to assess the effective number of walls contributing to the torsional stiffness of BNNTs.

Figure 2 shows the effective shear moduli for these two extreme cases, G_s (solid-rod case) and G_h (hollow-cylinder case), plotted as a function of the nanotube diameter d. For the nine nanotubes in the range d = 12−27 nm, G_h is markedly (up to 1 order of magnitude) larger than both reference values G_{th}(BNNT) and G_{exp}(*h*-BN). This indicates that the hollow-cylinder model is not appropriate and that our starting hypothesis is correct: boron nitride nanotubes, unlike carbon nanotubes, do exhibit a strong interlayer mechanical coupling. Moreover, in the same diameter range, we find that the solid-rod shear modulus G_s = 300 ± 100 GPa is similar to both G_{th}(BNNT) and G_{exp}(*h*-BN) within the experimental error (also taking into account that G_s is slightly underestimated by taking r_{in} = 0). This means that for these BNNTs most, if not all, of their layers do twist together in a correlated fashion, thereby making BNNTs up to 10 times torsionally stiffer than CNTs.[8]

Besides their high torsional stiffness, we were interested in probing the torsional strength of BNNTs. BNNTs were twisted repeatedly at angles up to 60°, in both directions, by pressing successively on both sides of the pedal (Figure 3). For each pressing, we observed an apparent softening of the system as the torsion angle increases. However, the pedal returned to its horizontal position after each cycle (Figure 3a,b), and the torque−torsion relation was found to be reproducible over time within the margin of experimental error (Figure 3c). These are clear indications that the deformation undergone by the nanotube remains elastic and that no plastic transition, let alone failure, has occurred. These phenomena were observed for all three nanotubes measured. A plausible explanation for the reversible softening observed at large angles is the progressive sliding of the BNNT outer layers with respect to the inner ones, a process similar to the stick−slip behavior previously observed with WS_2 nanotubes.[15] However, the latter displayed a reproducible pattern of periodic spikes, whereas BNNT torsion at large angles only shows random and irreproducible fluctuations (Figure 3c). Therefore, we believe that these fluctuations are rather due to noise (e.g., the AFM tip slipping along the pedal at large torsion angles) than to a well-defined stick-slip behavior.

Remarkably, unlike CNTs,[8] BNNTs do not break even after repeated twisting at large torsion angles. A lower estimate of BNNT torsional strength τ_{BNNT} can be calculated from the maximum load applied on the nanotube. The torsional strength is given by the maximal shear load applied before failure divided by the cross-section area, yielding $\tau_{BNNT} = T_{max}/(\pi r_{out}{}^3)$, where T_{max} is the maximum torque exerted on the nanotube. For the nanotube of Figure 3c, we find that τ_{BNNT} > 2.0 GPa, compared with τ_{CNT} = 0.14 and 0.19 GPa for the two CNTs studied in ref 8 (torsional strength calculated for the whole tube). The two other BNNTs investigated exhibited similar strengths (Table S1). BNNTs are therefore at least an order of magnitude torsionally stronger that CNTs. Similarly to what has been already observed in tensile tests,[25] the interlayer mechanical coupling enables a distribution of the load between layers and allows BNNTs to sustain torques much larger than CNTs of similar diameters without breaking.

Interestingly, the ultrahigh torsional stiffness of BNNTs described above is observed in a certain range of nanotube diameters. It can be seen in Figure 2 that the torsional stiffness

dx.doi.org/10.1021/nl303601d | *Nano Lett.* 2012, 12, 6347−6352

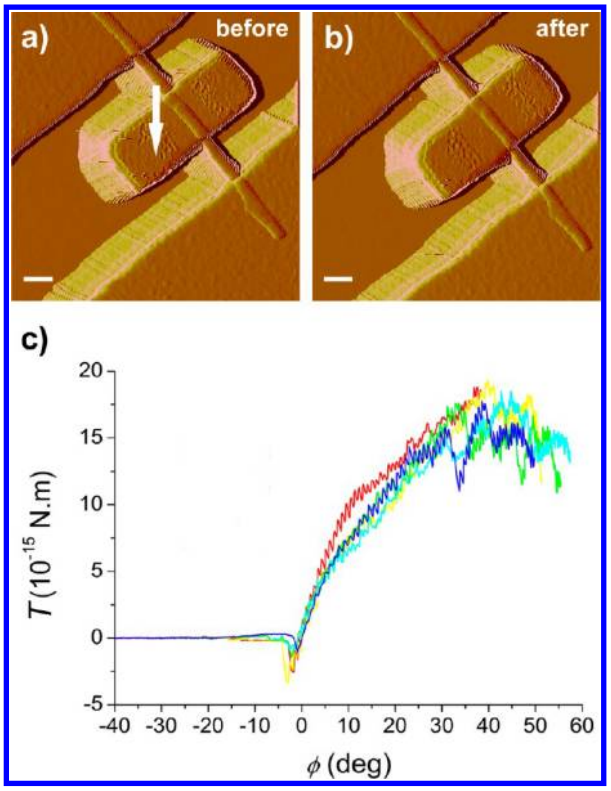

Figure 3. Nonlinear torsional behavior of multiwall BNNTs. AFM tapping mode amplitude images (a) before and (b) after repeated twisting at large torsion angle. The pedal is pressed on several times on one side with increasing torsion angles up to 60° (larger angles were not possible due to the geometry the AFM tip). The same procedure is then repeated on the other side and so on. After each pressing, the pedal remains horizontal, thereby indicating that the nanotube torsion remains elastic. Scale bars: 200 nm. (c) Torque plotted as a function of the torsion angle for the 1st (red), 5th (yellow), 15th (green), 29th (cyan), and 42th (blue) twisting cycle. The torque and torsion angles were calculated as in ref 8. Despite an apparent softening at large twisting angles, the torque–torsion relation is reproducible over time, which rules out a possible elastic–plastic transition.

of BNNTs significantly decreases for diameters smaller than 12 nm and larger than 27 nm, suggesting a decrease in the interlayer coupling. Surmising that the dependence of the interlayer coupling with nanotube diameter could be due to structural differences, we imaged multiwall BNNTs of various diameters using TEM (Figure 4a–c and Figure S2). The most striking feature is the presence of series of darker regions along the walls of multiwall BNNTs. Such high contrast areas have been observed previously and attributed to the presence on facets, which manifest themselves as polygonal cross section.[26−28] Remarkably, these features appear in most nanotubes with diameters above 12–15 nm but are absent in thinner BNNTs. It seems therefore that the onset of ultrahigh torsional stiffness correlates with the appearance of faceting.

We propose a theoretical model to rationalize the observed dependence of the torsional stiffness on BNNT diameter (see Figure 4d and Supporting Information). The transition between circular and faceted cross sections results from a delicate balance between intralayer and interlayer energy contributions. Interlayer contributions correspond to the stacking energy between shells. Because of their intrinsic curvature, there is a loss of registry between layers in circular multiwall BNNTs compared to the perfect eclipsed AA′ stacking of *h*-BN, and thus the interlayer energy increases. Faceting of the tube decreases the interlayer energy by improving the registry between walls (Figure 4d) but at the same time requires the formation of facet edges, which increases the intralayer energy. It can be shown (see Supporting Information) that intralayer energy scales like the number of layers, i.e., like the radius of the nanotube R, whereas interlayer energy scales like the cross-sectional area, i.e., like R^2. Consequently, when R increases, interlayer contributions dominate, and the faceted geometry becomes energetically favorable: when the nanotube becomes thick enough, it can create large flat areas with perfect registry that compensate the energy cost associated with the sharp edges. The high interaction energy between layers accounts for the appearance of facets in BNNTs,[26−28] whereas faceting has been only marginally observed in multiwall CNTs.[29] Upon twisting, facet edges are assumed to lock shells together, thereby giving rise to the observed correlation between the onset of ultrahigh stiffness and faceting.

A softening is observed for large BNNTs with diameters larger than 27 nm, even though TEM images clearly show them as faceted (see Figure 4c). We suggest that these nanotubes undergo partial or total "unfaceting" upon twisting, allowing the outer shells to slide around the inner ones. This assumption is supported by the fact that the torsional energy of one layer scales like R^3 (see Supporting Information), whereas the stabilization brought about by faceting scales like R^2. When the BNNT radius increases, torsion is expected to supply sufficient energy to the nanotube to revert it back to a cylindrical geometry. In addition, TEM images show that thick BNNTs are not pristine and exhibit interwall defects (Figure 4c). These defects consist of cavities, at the edge of which layers can be seen to fold on themselves in a hairpin-like fashion. Accumulation of such defects could impair the interlayer stacking and thus contribute to the relative softening observed for thick BNNTs. These cavities do not damage the BNNT intralayer mechanical properties and are thus not expected to entail nanotube failure. While the effects of both unfaceting and cavities might be involved in thick BNNTs, the systematic dependence of BNNT interlayer coupling on the nanotube diameter suggests that unfaceting is the main reason for the softening observed above 27 nm.

In summary, we have shown that in the 12–27 nm diameter range BNNTs behave as a strongly coupled material, where, unlike for CNTs, all layers contribute to the mechanical properties. Consequently, BNNTs reveal to be up to 1 order of magnitude torsionally stiffer and stronger that CNTs and exhibit exceptional torsional resilience. Owing to BNNTs ultrahigh stiffness and high mechanical coupling that locks layers together and limits internal friction, BNNT-based nanoresonators should benefit from both a higher resonance frequency and a higher quality factor than their carbon counterparts. Finally, the faceted nature of BNNTs, combined with their high interlayer sliding energy, high stiffness, and high strength, should make BNNTs an excellent material for the production of yarns,[30] fibers, and nanocomposites with outstanding mechanical properties.

■ ASSOCIATED CONTENT

Ⓢ Supporting Information

(1) Torsional spring constants and shear moduli for all nanotubes investigated; (2) additional plots of linear stiffness against lever arm (similar to Figure 1d) for several BNNTs; (3)

dx.doi.org/10.1021/nl303601d | *Nano Lett.* 2012, 12, 6347–6352

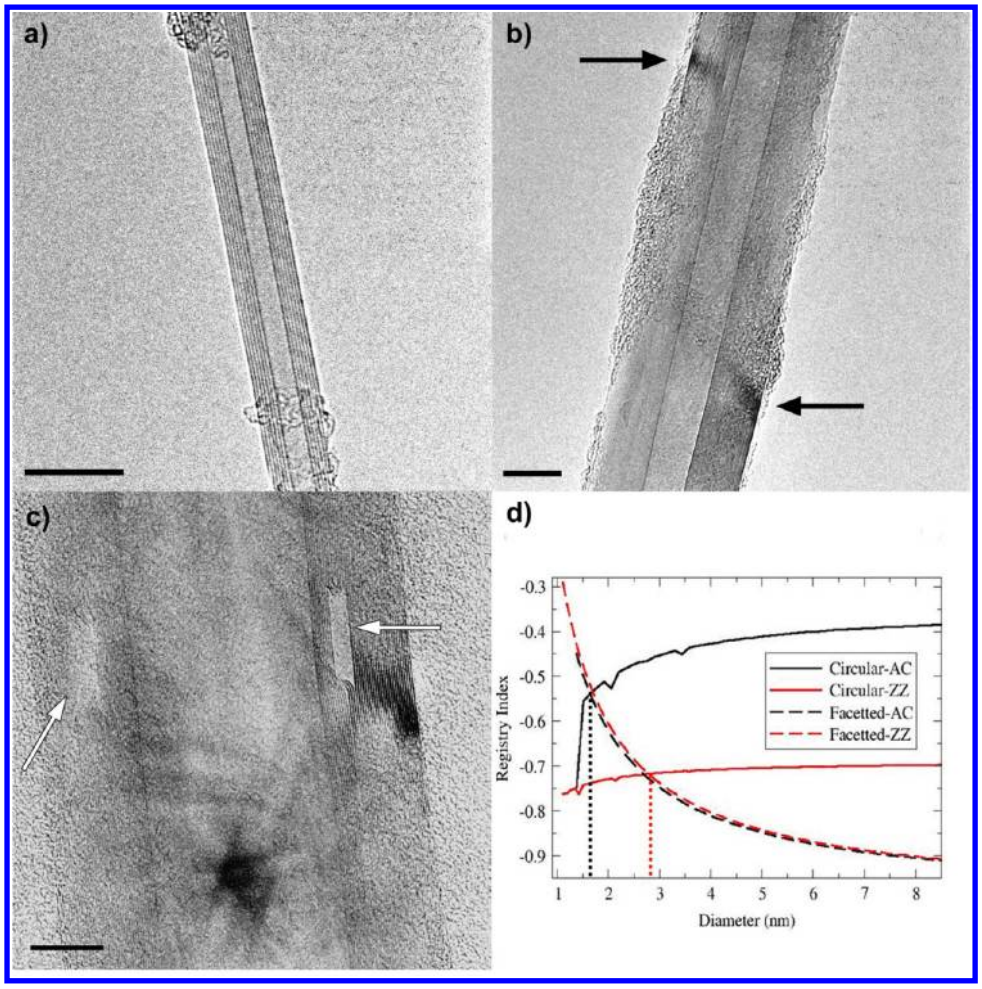

Figure 4. Structure and layer stacking of multiwall BNNTs. (a) Transmission electron microscopy (TEM) image of a thin BNNT (d = 7 nm). Scale bar: 10 nm. (b) TEM image of an intermediate BNNT (d = 25 nm). The dark areas denote the presence of facets, i.e., polygonal cross sections. Scale bar: 10 nm. (c) TEM image of a thick BNNT (d = 38 nm). The white arrows point at cavities located inside the nanotube walls. The presence of these defects could degrade the mechanical properties of BNNT with large diameters (d > 27 nm). Scale bar: 10 nm. (d) Optimal registry index (RI) as a function of outer wall diameter for (n, n)@(n + 5, n + 5) armchair (black lines) and (n, 0)@(n + 9, 0) zigzag (red lines) double-wall BNNTs with circular (solid lines) and faceted (dashed lines) cross sections (see Supporting Information for details). The RI is parameter which quantifies the degree of interlayer commensurability in layered materials. It is a real number bound in the range [−1, +1] where −1 stands for perfect registry (i.e., AA′ stacking where a boron atom in one layer resides atop a nitrogen atoms in adjacent layers and vice versa) and +1 stands for worst registry (i.e., AA stacking where boron and nitrogen atoms in one layer are fully eclipsed with their counterparts in adjacent layers).[20,31] As soon as d > 2−3 nm, the stacking is better for faceted than circular nanotubes.

TEM images of BNNTs of different diameters and various cross-section geometry; (4) materials and methods: synthesis; nanofabrication; BNNT torsion measurements; microscopy; (5) modeling: details of registry index calculations for a faceted double-walled BNNT; scaling of torsional mechanical coupling with BNNT radius. This material is available free of charge via the Internet at http://pubs.acs.org.

AUTHOR INFORMATION

Corresponding Author

*E-mail: ernesto.joselevich@weizmann.ac.il.

Present Address

[⊥]GE India Technology Centre, Bangalore 560066, India.

Notes

The authors declare no competing financial interests.

ACKNOWLEDGMENTS

This work was supported by the Israel Science Foundation, the Israeli Ministry of Defense, the Minerva Foundation, the Kimmel Center for Nanoscale Science and Moskowitz Center for Nano and Bio-Nano Imaging at the Weizmann Institute, and the Djanogly, Alhadeff, and Perlman foundations, as well as the Center for Nanoscience and Nanotechnology at Tel-Aviv University, the Humboldt Foundation, and the Lise Meitner-Minerva Center for Computational Quantum Chemistry. J.G. is partly supported by the French Ministry of Foreign Affairs. C.Z., Y.B., and D.G. are grateful to WPI Center for Materials Nanoarchitectonics (MANA) tenable at the National Institute for Materials Science (NIMS), Tsukuba, Japan, for a long-term support of the BN nanotube synthesis project. We thank L. Kronik, M. Bar-Sadan, and R. Tenne for helpful discussions.

REFERENCES

(1) Yu, M.-F.; Lourie, O.; Dyer, M. J.; Moloni, K.; Kelly, T. F.; Ruoff, R. S. *Science* **2000**, *287*, 637−640.

(2) Peng, B.; Locascio, M.; Zapol, P.; Li, S.; Mielke, S. L.; Schatz, G. C.; Espinosa, H. D. *Nat. Nanotechnol.* **2008**, *3*, 626−631.
(3) Koziol, K.; Vilatela, J.; Moisala, A.; Motta, M.; Cunniff, P.; Sennett, M.; Windle, A. *Science* **2007**, *318*, 1892−1895.
(4) Coleman, J. N.; Khan, U.; Gun'ko, Y. K. *Adv. Mater.* **2006**, *18*, 689−706.
(5) Hierold, C.; Jungen, A.; Stampfer, C.; Helbling, T. *Sens. Actuators, A* **2007**, *136*, 51−61.
(6) Cumings, J.; Zettl, A. *Science* **2000**, *289*, 602−604.
(7) Williams, P.; Papadakis, S.; Patel, A.; Falvo, M.; Washburn, S.; Superfine, R. *Phys. Rev. Lett.* **2002**, *89*, 255502.
(8) Cohen-Karni, T.; Segev, L.; Srur-Lavi, O.; Cohen, S. R.; Joselevich, E. *Nat. Nanotechnol.* **2006**, *1*, 36−41.
(9) Salvetat, J.-P.; Briggs, G. A. D.; Bonard, J.-M.; Bacsa, R. R.; Kulik, A. J.; Stöckli, T.; Burnham, N. A.; Forró, L. *Phys. Rev. Lett.* **1999**, *82*, 944−947.
(10) Bourlon, B.; Glattli, D. C.; Miko, C.; Forro, L.; Bachtold, A. *Nano Lett.* **2004**, *4*, 709−712.
(11) Jiang, H.; Yu, M. F.; Liu, B.; Huang, Y. *Phys. Rev. Lett.* **2004**, *93*, 185501.
(12) Papadakis, S.; Hall, A.; Williams, P.; Vicci, L.; Falvo, M.; Superfine, R.; Washburn, S. *Phys. Rev. Lett.* **2004**, *93*, 146101.
(13) Nam, C.-Y.; Jaroenapibal, P.; Tham, D.; Luzzi, D. E.; Evoy, S.; Fischer, J. E. *Nano Lett.* **2006**, *6*, 153−158.
(14) Nagapriya, K.; Berber, S.; Cohen-Karni, T.; Segev, L.; Srur-Lavi, O.; Tománek, D.; Joselevich, E. *Phys. Rev. B* **2008**, *78*, 165417.
(15) Nagapriya, K.; Goldbart, O.; Kaplan-Ashiri, I.; Seifert, G.; Tenne, R.; Joselevich, E. *Phys. Rev. Lett.* **2008**, *101*, 195501.
(16) Kaplan-Ashiri, I.; Cohen, S. R.; Gartsman, K.; Rosentsveig, R.; Seifert, G.; Tenne, R. *J. Mater. Res.* **2004**, *19*, 454−459.
(17) Chopra, N. G.; Luyken, R. J.; Cherrey, K.; Crespi, V. H.; Cohen, M. L.; Louie, S. G.; Zettl, A. *Science* **1995**, *269*, 966−967.
(18) Golberg, D.; Bando, Y.; Huang, Y.; Terao, T.; Mitome, M.; Tang, C.; Zhi, C. *ACS Nano* **2010**, *4*, 2979−2993.
(19) Celik-Aktas, A.; Zuo, J. M.; Stubbins, J. F.; Tang, C.; Bando, Y. *Appl. Phys. Lett.* **2005**, *86*, 133110.
(20) Marom, N.; Bernstein, J.; Garel, J.; Tkatchenko, A.; Joselevich, E.; Kronik, L.; Hod, O. *Phys. Rev. Lett.* **2010**, *105*, 046801.
(21) Huang, Y.; Lin, J.; Tang, C. C.; Bando, Y.; Zhi, C. Y.; Zhai, T. Y.; Dierre, B.; Sekiguchi, T.; Golberg, D. *Nanotechnology* **2011**, *22*, 145602.
(22) Tang, C.; Bando, Y.; Sato, T.; Kurashima, K. *Chem. Commun.* **2002**, 1290−1291.
(23) Chowdhury, R.; Wang, C. Y.; Adhikari, S.; Scarpa, F. *Nanotechnology* **2010**, *21*, 365702.
(24) Bosak, A.; Serrano, J.; Krisch, M.; Watanabe, K.; Taniguchi, T.; Kanda, H. *Phys. Rev. B* **2006**, *73*, 041402.
(25) Wei, X.; Wang, M.-S.; Bando, Y.; Golberg, D. *Adv. Mater.* **2010**, *22*, 4895−4899.
(26) Golberg, D.; Mitome, M.; Bando, Y.; Tang, C. C.; Zhi, C. Y. *Appl. Phys. A: Mater. Sci. Process.* **2007**, *88*, 347−352.
(27) Celik-Aktas, A.; Zuo, J.-M.; Stubbins, J. F.; Tang, C.; Bando, Y. *Acta Crystallogr., A* **2005**, *61*, 533−541.
(28) Golberg, D.; Costa, P. M. F. J.; Lourie, O.; Mitome, M.; Bai, X.; Kurashima, K.; Zhi, C.; Tang, C.; Bando, Y. *Nano Lett.* **2007**, *7*, 2146−2151.
(29) Liu, M. *Carbon* **1994**, *32*, 393−403.
(30) Smith, M. W.; Jordan, K. C.; Park, C.; Kim, J.-W.; Lillehei, P. T.; Crooks, R.; Harrison, J. S. *Nanotechnology* **2009**, *20*, 505604.
(31) Hod, O. *Isr. J. Chem.* **2010**, *50*, 506−514.

Supporting Information

Ultrahigh Torsional Stiffness and Strength of Boron Nitride Nanotubes

Jonathan Garel,[†] *Itai Leven,*[‡] *Chunyi Zhi,*[§] *K.S. Nagapriya,*[†,⊥] *Ronit Popovitz-Biro,*[‖] *Dmitri Golberg,*[§] *Yoshio Bando,*[§] *Oded Hod,*[‡] *and Ernesto Joselevich**[,†]

[†]Department of Materials and Interfaces, Weizmann Institute of Science, Rehovot 76100, Israel

[‡]School of Chemistry, The Sackler Faculty of Exact Sciences, Tel Aviv University, Tel Aviv 69978, Israel

[§]International Center for Materials Nanoarchitectonics (MANA), National Institute for Materials Science (NIMS), Namiki 1-1, Tsukuba, Ibaraki 305-0044, Japan

[‖]Chemical Research Support, Weizmann Institute of Science, Rehovot 76100, Israel

*email: ernesto.joselevich@weizmann.ac.il

Table S1: BNNT torsional mechanical characterization.

BNNT #	d (nm)	L (nm)	κ (10^{-14} N.m)	G_s (GPa)	G_h (GPa)	τ_{BNNT}(GPa)
A	10.5 ± 0.3	100 ± 10	0.17 ± 0.07	130 ± 60	530 ± 220	
B	10.7 ± 0.9	100 ± 20	0.25 ± 0.07	190 ± 80	770 ± 290	
C	13.4 ± 1.1	170 ± 30	0.9 ± 0.3	460 ± 180	2300 ± 800	
D	17.6 ± 0.7	320 ± 10	1.2 ± 0.2	420 ± 80	2600 ± 500	
E	17.8 ± 1.5	380 ± 10	0.6 ± 0.2	210 ± 90	1400 ± 600	
F	18.5 ± 1.0	420 ± 10	0.8 ± 0.2	300 ± 70	2100 ± 500	
G	21.6 ± 1.4	290 ± 30	1.3 ± 0.3	180 ± 50	1400 ± 400	> 0.8
H	22.4 ± 0.8	210 ± 10	3.1 ± 0.5	260 ± 50	2200 ± 400	> 2.0
I	22.8 ± 0.6	350 ± 10	1.6 ± 0.2	210 ± 40	1800 ± 300	
J	25.4 ± 1.2	320 ± 10	4.3 ± 0.7	340 ± 80	3200 ± 700	
K	26.0 ± 2.2	330 ± 10	3.3 ± 0.8	240 ± 80	2300 ± 800	> 1.3
L	27.7 ± 1.0	370 ± 10	2.3 ± 0.3	150 ± 30	1500 ± 300	
M	29.6 ± 2.6	180 ± 20	3.5 ± 0.2	82 ± 20	910 ± 180	
N	30.2 ± 2.4	280 ± 10	1.7 ± 0.3	58 ± 14	660 ± 150	
O	32.6 ± 0.7	360 ± 20	1.1 ± 0.2	36 ± 9	440 ± 110	
P	39.2 ± 2.0	290 ± 30	6 ± 2	63 ± 27	920 ± 390	
Q	42.8 ± 3.6	280 ± 20	4.9 ± 0.7	41 ± 10	660 ± 150	

d: BNNT diameter; L: BNNT suspended length (obtained both from AFM topography); κ: torsional spring constant; G_s and G_h: effective shear moduli according to solid rod and hollow cylinder model, respectively; $\tau_{\mathrm{BNNT:}}$ torsional strength (calculated for the whole nanotube). The experimental error (EE) for d is the standard deviation of several measurements performed along the BNNT length. The EE for L is derived from the resolution of the AFM topography image. The EE for κ is the damped least-squares fitting error obtained by fitting linear stiffness versus lever arm plots (Figure 1d and Figure S1) to equation (1) (see text and Methods below). The EE for G_h and G_s is obtained by combining the EE for d, L and κ.

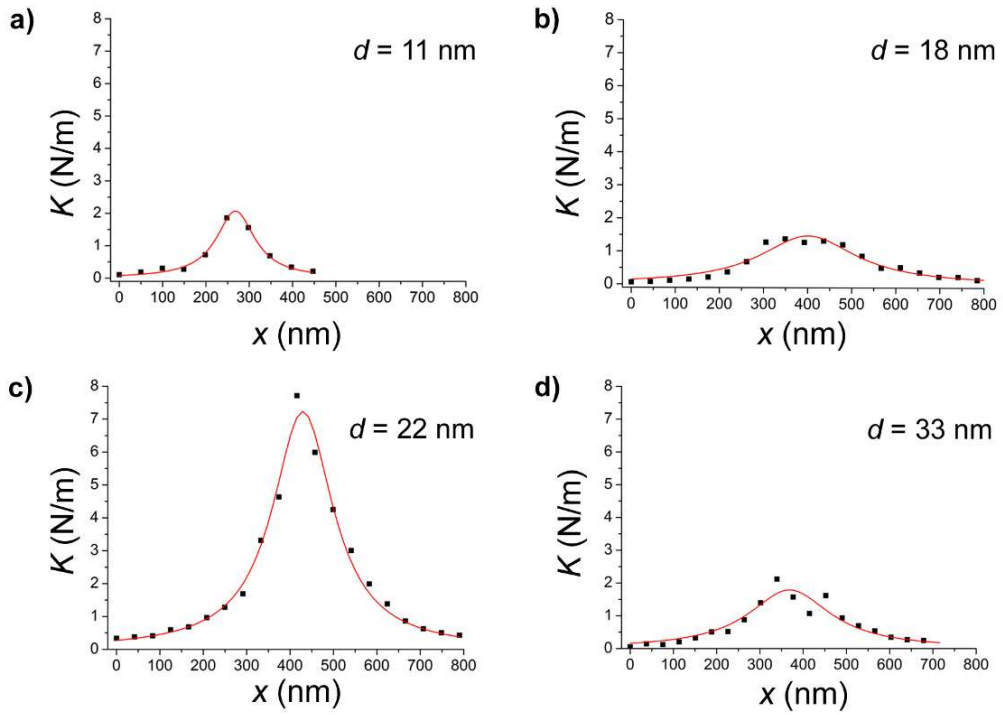

Figure S1: Additional plots of linear stiffness against lever arm, for nanotubes B **(a)**, D **(b)**, H **(c)** and O **(d)**. *x* represents the position along the pedal (the first measurement point is set to zero by definition). The data were fitted to equation (1) (see text).

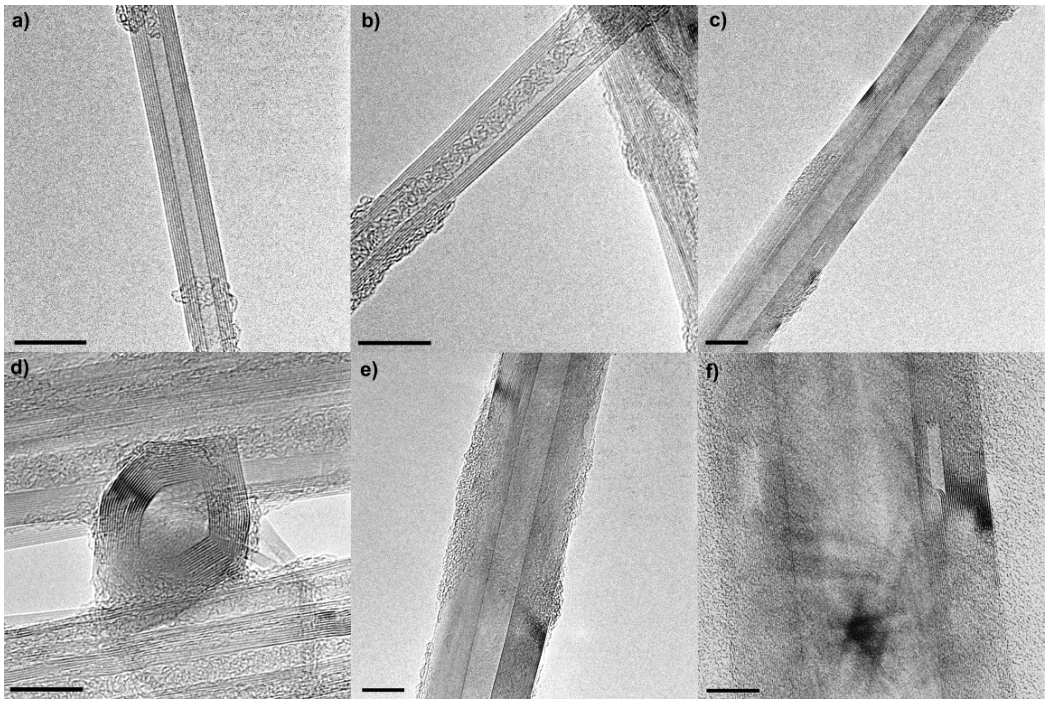

Figure S2: BNNTs of different diameters and cross-section geometry. TEM images of BNNTs of diameters 7 nm **(a)**, 9 nm **(b)**, 16 nm **(c)**, 22 nm **(d)**, 25 nm **(e)**, and 37 nm **(f)**. Whereas nanotubes **(a)** and **(b)** have circular cross-sections, the black areas visible in nanotubes **(c)**, **(e)** and **(f)** are a known indication of faceting. The faceted nature of nanotube **(d)** can be demonstrated by a direct observation of its polygonal cross-section. All scale bars: 10 nm.

Methods

Synthesis: BNNT were synthesized by chemical vapor deposition as described in [S1] (nanotubes A to C) and [S2] (nanotubes D to Q).

Nanofabrication: The torsional BNNT-based NEMS were produced by methods similar to those reported for previous torsional devices.[S3-S5] Alignment marks were created on thermally oxidized silicon wafers (Si<100>, oxide thickness: 1μm) by electron-beam lithography, metal evaporation and lift-off. BNNTs were dispersed in 1,2-dichloroethane by brief sonication prior to deposition. BNNTs tend to agglomerate as bundles and could not be fully separated by sonication. To produce individual nanotubes, BNNT aggregates were deposited on the Si wafer, which was then flushed with acetone and isopropanol, leaving behind several well separated nanotubes suitable for device production. The nanotubes were mapped and their diameter was measured by AFM imaging. Pads and pedals were laid down respectively onto the ends and middle part of the selected BNNTs by electron beam lithography, electron beam evaporation of Cr (5 nm) and Au (80 nm), and lift-off in acetone. The SiO_2 layer was then etched in aqueous HF/NH_4F (1:6) for 7 minutes. Then, without drying the samples, the etching solution was consecutively replaced by water, ethanol and pressurized CO_2, from which they were critical-point dried. Devices A, B and C (Supplementary Table 1) were grounded during the torsion experiment, which required additional fabrication steps. Large electrodes were written

by electron-beam lithography together with pads and pedals. Then, before etching the SiO_2 layer, the sample was mounted into a chip carrier and wire-bonded.

BNNT torsion measurements: AFM imaging and mechanical measurements were performed on a Veeco Multimode/Nanoscope V equipped with a closed-loop scanner.

The device on which we wish to perform the torsion experiment is first imaged in tapping mode (TM) AFM. We then zoom at the desired position and press on the pedal with the AFM tip, which twists the nanotube. During each press cycle, we acquire measurements of both the oscillation amplitude of the cantilever and its TM deflection as a function of its z-position ("force-distance measurement"). The TM deflection plot records the deformation of the cantilever as it presses on the pedal, whereas the amplitude plot is used as a control: when the tip touches the pedal, the oscillation amplitude of the cantilever is supposed to reach zero. Before the experiment itself, we always perform a force-distance measurement on a hard Au surface as a calibration (Figure S3). In order to get meaningful data, we need the spring constant of the cantilever to be of the same order of magnitude as the apparent spring constant of the nanotube. In most cases, 70 kHz silicon tips (Olympus) with a spring constant of ~ 2 N/m were successfully used; for devices A, B and C, we used low-frequency cantilevers (Micromasch, ν = 20 kHz, k_c = 0.3 N/m). All spring constants were recalibrated by thermal tuning method. Additionally, the whole experiment is conducted under dry N_2 flow in order to reduce humidity and thermal fluctuations. For thin BNNT devices (devices A, B and C), both the tip and the device were grounded during the experiment, in order to avoid static charging, which could break the device through electrostatic forces.

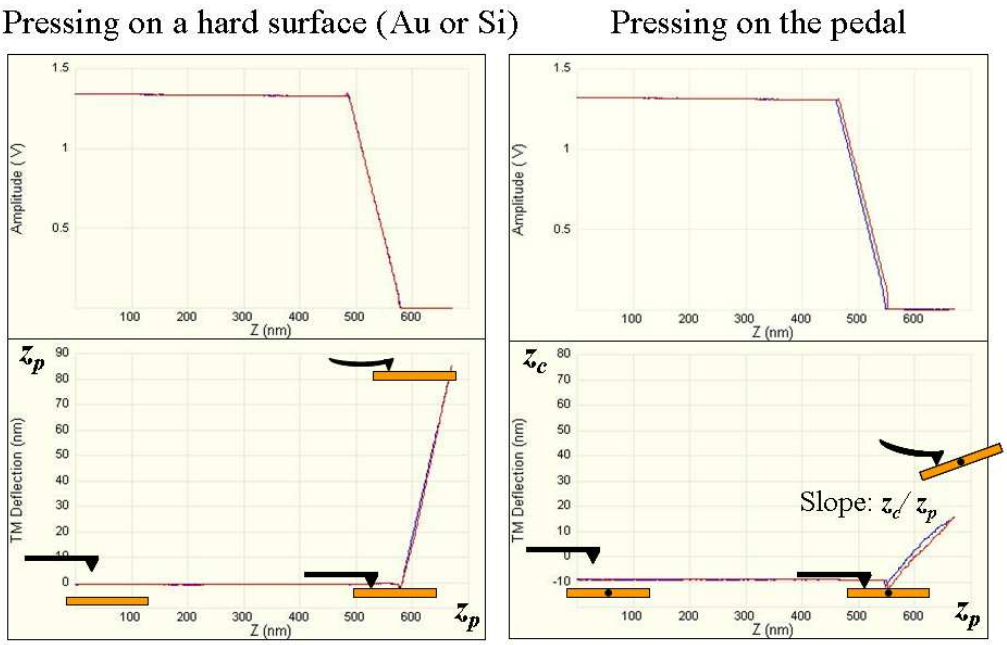

Figure S3: Force-distance measurements recorded upon pressing on a hard surface (left) and on the pedal (right). In both cases, when the tip touches the surface, the tapping amplitude reaches zero. The tapping mode deflection then increases linearly, corresponding to cantilever deformation. Because the pedal twists, the deformation undergone by the cantilever is less significant than if pressing on a hard surface, hence the smaller slope. In blue: trace; in red: retrace.

The torsional stiffness was measured by pressing at a series of points along the pedal as described in the text, in Figure 1d, and in Supplementary Figure 1. Since k_c, z_p and z_c (see text) can all be determined with accuracy < 2%, the major source of uncertainty on κ comes from the experimental fit. Additionally, we were cautious to reach only low torsion angles (< 20°), in order to avoid any non-linear response, or plastic transition, which could arise at higher torsion angles. In most cases, the measurements were repeated either immediately, or a few weeks after the first

experiment. The values measured for κ were found to be identical within the margin of experimental error. This indicates that no plastic irreversible transition has occurred, and that the true elastic torsional spring constant of each BNNT device is obtained.

We were concerned that the metallic pedal might undergo deformation upon pressing, thus leading to an underestimation of the torsional spring constant. To test this possible effect, we built several "diving boards" (cantilevers extending from the metallic pads) and pressed along the board at regular intervals while acquiring force-distance measurements. We then plotted the stiffness as a function of the distance from the edge (Figure S4). It is visible that while the stiffness indeed decreases along the board, thus indicating that it undergoes deformation, the board always remains much stiffer than the "pedal + nanotube" system. We could measure the apparent torsional spring constant of the board to be $\kappa_{Au} = 1.9 \pm 0.1 \cdot 10^{-12}$ N·m, which is one to two orders of magnitude larger than the typical spring constant of a multiwall BNNT. Therefore, in most cases, the elasticity of the Au pedal was negligible. When deemed necessary, we corrected the nanotube torsional spring constants accordingly.

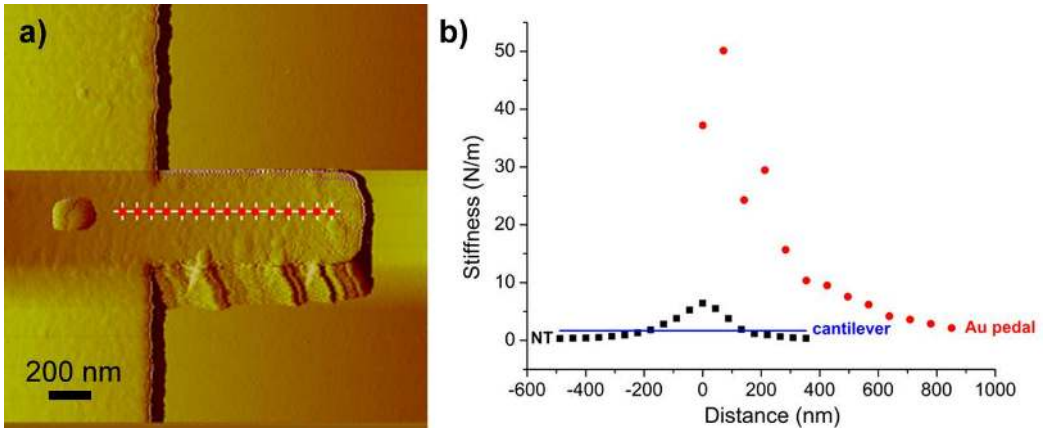

Figure S4: Pedal deformation. (a) AFM tapping mode image of a suspended "diving board". For every position marked with a red dot, we acquired a force-distance measurement. **(b)** Relative stiffness of a BNNT (black) compared to Au pedal (red) and AFM cantilever stiffness (blue), as a function of distance from the torsional axis. Whereas the nanotube and cantilever stiffness are of the same order of magnitude, the Au pedal is one to two orders of magnitude stiffer.

Microscopy: SEM imaging was performed with a Supra 55VP FEG LEO Zeiss in ultra-high vacuum, at acceleration voltage 5 kV. TEM imaging was performed on a FEI/Philips CM120, at acceleration voltage 120 kV.

Modeling

1. Registry index for a faceted double walled boron nitride nanotube

A faceted achiral double walled boron nitride nanotube (DWBNNT) has a polygonal cross-section which can be represented as follows (we use a perfect hexagonal cross section as an example):

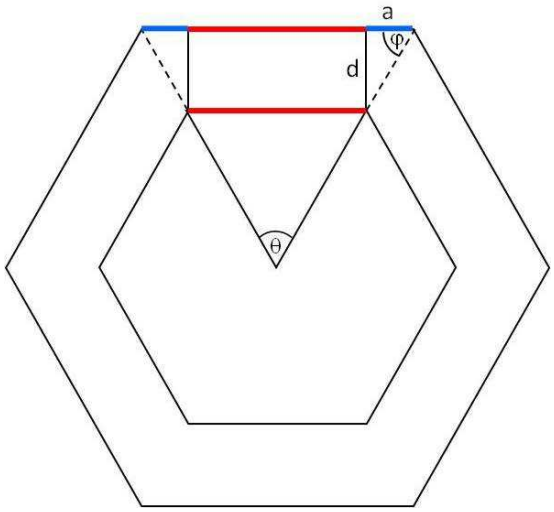

Figure S5: Model for a faceted nanotube with a hexagonal cross section

We identify two types of regions along the polygonal circumference: (i) Side regions where sections of the outer prism can be projected onto parallel sections of the inner prism (we shall name these sections as "red" sections as they are marked with bold red lines in the above figure) (ii) Apex regions where such projections are not possible (these sections will be named as blue sections as they are marked with bold blue lines

in the figure). The length of each of the "blue" apex section is $a = d / \tan\varphi$ where $d \approx$ 3.33 Å is the interlayer separation. The angle φ is related to the central angle $\theta = 2\pi/n$, and thus to the number of apexes n, via $\varphi = \frac{\pi - \theta}{2} = \pi\left(\frac{1}{2} - \frac{1}{n}\right)$. Using these relations we find that the total length of the "blue" sections of the outer shell is given by $2an = \frac{2dn}{\tan\left[\pi\left(\frac{1}{2} - \frac{1}{n}\right)\right]}$.

The overall circumference of the outer shell L is assumed to be equal to the circumference of the corresponding pristine tube namely, $L = \pi D$, D being the diameter of the non-faceted outer tube. Therefore, the portion of the circumference that is of "red" type:

$$\beta = \frac{L - 2an}{L} = 1 - \frac{2dn}{\pi D \tan\left[\pi\left(\frac{1}{2} - \frac{1}{n}\right)\right]}$$

For the calculation of the registry index we now assume that the "red" sections are in perfect registry and thus contribute "-1" to the overall registry index and the "blue" sections which have no interlayer overlap are "neutral" in terms of their registry mismatch and thus contribute "0" to the overall registry. Thus the registry index can now be evaluated as:

$$RI_{Facetted} = (-1)\cdot\beta + (0)\cdot(1-\beta) = -\beta = \frac{2dn}{\pi D \tan\left[\pi\left(\frac{1}{2} - \frac{1}{n}\right)\right]} - 1$$

It should be noted that in order to obtain perfect registry in the "red" regions the difference in length between the inner and outer facet which is of length $2a$ should be

integer multiples of the unit cells translational vector along the nanotube circumference. Naturally, this condition is hard to achieve and therefore one should expect that the "blue" regions will be somewhat stressed to allow for enhanced registry in the "red" regions which will not be in perfect registry.

Figure 4d presents the results of this model for a hexagonal cross section. The dependence of the registry index, calculated using the above described procedure, on the number of apexes of the faceted nanotubes is plotted in Figure S6.

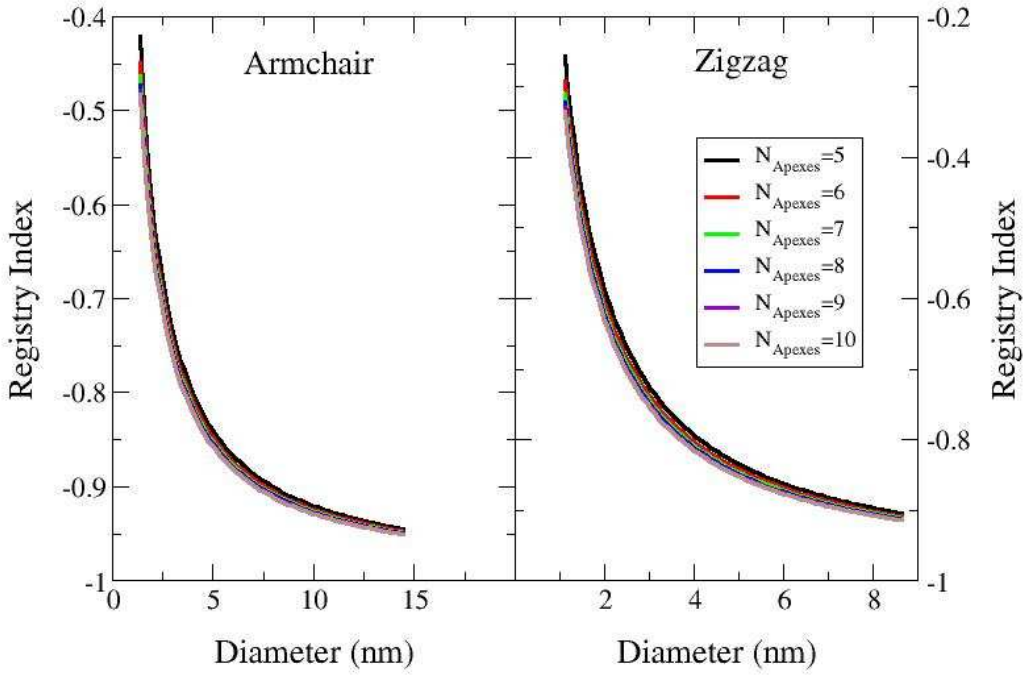

Figure S6: Dependence of the registry index of a faceted BNNT, calculated using the procedure described above, on the number of apexes of the faceted nanotubes. Left panel: armchair DWBNNTs; Right panel: zigzag DWBNNTs. As can be seen, the dependence of the calculated RI on the number of apexes is relatively weak thus justifying our use of a hexagonal cross section.

2. Scaling of torsional mechanical coupling with BNNT radius

TEM imaging indicated that faceting is the origin of the ultrahigh torsional stiffness observed in multiwall BNNTs. Based on the observation that thick BNNTs appear faceted in TEM and yet exhibit weak torsional coupling, we hypothesized that thick BNNTs undergo unfaceting upon twisting: under torsion, some (or all) shells of a thick BNNT undergo a conformational change that allows the outer layer(s) to slide freely.

The model we develop addresses the two following questions:

(i) What drives the formation of facets, and why do they appear only above a certain diameter?

(ii) What drives the unfaceting of faceted nanotubes? Why is it favored for thicker tubes?

This model is based primarily on analyzing how each contribution to the BNNT total energy scales with the BNNT radius R.

2.1. Formation of facets

The faceting of the nanotubes, namely the transition between circular and faceted cross sections, results from a delicate balance between intralayer and interlayer energy contributions. We will now evaluate the scaling with R of intralayer and interlayer effects both for cylindrical and faceted nanotubes.

2.1.1. Intralayer energy

The intralayer energy for circular nanotubes corresponds to the curvature strain energy E_{curv}. E_{curv} scales linearly with the number of layers, and quadratically with the curvature of the nanotube.[S6] The number of layers scales with R and the curvature scales with R^{-1}, therefore $E_{curv} \propto R^{-1}$.

The intralayer energy for faceted nanotubes corresponds to the energy required to create facet edges. E_{edges} is proportional to the total number of edges. The number of edges per layer being a constant, E_{edges} therefore increases linearly with the number of layers: $E_{edges} \propto R$.

2.1.2. Interlayer energy

The interlayer energy corresponds to the attraction (or repulsion) felt by an atom from its nearest out-of-plane neighbors. The total interlayer energy E_{inter} is the sum of these individual contributions over the whole nanotube. E_{inter} therefore scales like the nanotube cross-section area, i.e. $E_{inter} \propto R^2$, both for circular and faceted nanotubes.

E_{inter} also depends on the stacking between the layers: the better the stacking, the lower (i.e. the more stabilizing) E_{inter} will be. Or, expressed in terms of registry index (RI) (see Figure 4d): the lower the RI, the lower E_{inter}. Figure 4d shows that for a diameter d > 2-3 nm, the RI is lower for faceted than for circular nanotubes. One can therefore safely assume that for our BNNTs, E_{inter} is lower for faceted than for

circular nanotubes. Moreover, the RI saturates and does not vary with d when d becomes larger than a few nm.

2.1.3. Total energy

One can now express the total energy of the nanotube, both in the faceted and the circular geometry. For circular nanotube, the total energy E^C can be written as

$$E^C(R) = E^C_{inter}(R) + E^C_{intra}(R) = \alpha R^2 + \beta R^{-1}$$

where α and β are independent of R. Similarly, for faceted nanotubes:

$$E^F(R) = E^F_{inter}(R) + E^F_{intra}(R) = \alpha' R^2 + \beta' R$$

where α' and β' are independent of R. We have also established that $E^F_{inter} < E^C_{inter}$ and therefore $\alpha' < \alpha$. As R increases, interlayer contributions, which scale like R^2, become dominant over intralayer contributions, which scale like R or R^{-1}. Since $E^F_{inter} < E^C_{inter}$, the energy of the faceted geometry becomes lower than the energy of the cylindrical geometry above a certain R_F (faceting radius): the nanotube undergoes faceting. In other words, when the nanotube becomes large enough, it can create large flat areas with perfect registry that compensate for the energetical cost of edges; then faceting occurs.

2.2. Unfaceting under torsional stress

Upon application of a torque, a third energy contribution must be considered: the elastic torsional energy E_{twist}. Let us now evaluate the scaling of E_{twist} with R in the

two extreme cases described in the main text of the article (one layer twisting and slipping vs. all layer twisting together).

One layer twisting: $E_{twist\text{-one}} = (1/2)\kappa_{one}\phi^2$ where $\kappa_{one} = (4G\pi R^3\delta r)/(2L)$: $E_{twist\text{-}one} \propto R^3$.

All layers twisting: $E_{twist\text{-all}} = (1/2)\kappa_{all}\phi^2$ where $\kappa_{one} = (G\pi R^4)/(2L)$: $E_{twist\text{-}all} \propto R^4$.

Therefore, torsional energy terms, which scale at least as R^3, are expected to become dominant over both intra- and interlayer energy terms (scaling at most as R^2) as R increases. Since $E_{twist\text{-}one} \propto R^3$ and $E_{twist\text{-}all} \propto R^4$, slipping of the outer layer around the inner shells should become favorable for large R – even at the expense of significant internal reorganization and increase of the interlayer energy. In other words: above a certain R_U (unfaceting radius) and submitted to a torsional stress, the faceted nanotube reverts back to a circular geometry, thereby allowing its outer shell to freely slide around its inner layers. It should be noted that unfaceting is also expected to occur below R_U if the torsion angle is large enough, which probably accounts for the relative softening observed at large twisting angles in Figure 3.

2.3. Summary

We have shown here that the various torsional behaviors observed for BNNTs are due to a delicate balance of their intralayer, interlayer and torsional energies.

For thin nanotubes, intralayer energy dominates: the energetical cost of facet edges is too heavy and thin BNNTs are thus circular. They exhibit a low torsional coupling and low sliding energy, due probably to the loss of commensurability between layers arising when *h*-BN folds into BNNTs.

For intermediate nanotubes, interlayer energy dominates: interlayer stabilization allows the formation of faceted nanotube, and the preservation of the faceted structure upon twisting. A large torsional coupling ("ultrahigh stiffness") is observed.

For thick nanotubes, torsional energy dominates, entailing unfaceting of the nanotube to allow the outer shell to slip around the inner layers. The torsional coupling is again low.

Supplementary references

S1. Huang, Y.; Lin, J.; Tang, C. C.; Bando, Y.; Zhi, C. Y.; Zhai, T. Y.; Dierre, B.; Sekiguchi, T.; Golberg, D. *Nanotechnology* **2011,** *22,* 145602.

S2. Tang, C.; Bando, Y.; Sato, T.; Kurashima, K. *Chem. Commun.* **2002**, 1290-1291.

S3. Cohen-Karni, T.; Segev, L.; Srur-Lavi, O.; Cohen, S. R.; Joselevich, E. *Nature Nanotechnol.* **2006,** *1*, 36-41.

S4. Nagapriya, K.; Berber, S.; Cohen-Karni, T.; Segev, L.; Srur-Lavi, O.; Tománek, D.; Joselevich, E. *Phys. Rev. B* **2008,** *78,* 165417

S5. Nagapriya, K.; Goldbart, O.; Kaplan-Ashiri, I.; Seifert, G.; Tenne, R.; Joselevich, E. *Phys. Rev. Lett.* **2008,** *101,*195501.

S6. Srolovitz, D.; Safran, S.; Tenne, R. *Phys. Rev. E* **1994,** *49*, 5260-5270.